Defect identification using the core-electron contribution in Doppler-broadening spectroscopy of positron-annihilation radiation

S. Szpala, P. Asoka-Kumar, B. Nielsen, J. P. Peng, S. Hayakawa, and K. G. Lynn
Department of Physics, Brookhaven National Laboratory, P.O. Box 5000, Upton, New York 11973

H.-J. Gossmann
AT&T Bell Laboratories, 600 Mountain Avenue, Murray Hill, New Jersey 07974
(Received 22 December 1995; revised manuscript received 16 April 1996)

Reduction of background using a coincidence-detection system in Doppler-broadening spectroscopy of positron-annihilation radiation allows us to examine the contribution of high-momentum core electrons. The contribution is used as a fingerprint to identify chemical variations at a defect site. The technique is applied to study a variety of open volume defects in Si, including decorated vacancies associated with doping. [S0163-1829(96)03732-0]

I. INTRODUCTION

Point defects play an important role in electrical properties of semiconducting materials and there has been a significant effort to characterize them. In the concentration range of 10^{15} cm^{-3}, positron annihilation spectroscopy[1,2] (PAS) is one of very few methods of defect detection and this is due to the high affinity of positrons to open volume defects. Several observables are employed in PAS to characterize defects: positron lifetime, two-dimensional angular correlation radiation (2D-ACAR), positronium (Ps) formation, and Doppler broadening.[3] Positron lifetime experiments are capable of distinguishing different kinds of vacancies, due to vacancy-impurity binding, but provide no direct information on chemical variations.[4] 2D-ACAR (Ref. 5) data allow one to characterize defects through the analysis of the momentum distribution of conduction- and valence-band electrons in the perturbing fields of defects. However, interpretation of 2D-ACAR results requires detailed calculations of positron wave functions and the electronic band structure. Ps formation can be used to detect the presence of voids and variations at the surface, as well as at buried interfaces.[6] However, the Ps signal is not sensitive to point defects. Doppler broadening of annihilation radiation provides a sensitive method of defect characterization by measuring the momentum distribution of the electrons. Unlike 2D-ACAR, sensitive mainly to low-momentum electrons, it allows one to examine high-momentum core electrons. The core electrons of the atoms near a defect site retain the properties of the free atoms, including the momentum distribution. An impurity atom may have the distribution of the momentum of electrons distinct from the host atoms and the difference can be used to identify foreign atoms decorating vacancy sites.[7]

The principle of the method lies in the analysis of the positron annihilation line shape, which directly corresponds to the distribution of momentum of electron-positron pairs. The momentum itself is measured from the amount of the Doppler shift of the emitted photons. The photon energy in the laboratory frame differs from the center of mass frame by $\Delta E = -E_B/2 \pm cp_z/2$, where E_B is, approximately, the binding energy of electrons to the solid and p_z is the projection of the momentum of an electron-positron pair onto the photon direction. Since the majority of the annihilation events take place after positron thermalization, its momentum contribution to p_z may be neglected, compared to the high momentum of core electrons. The momentum distribution of core electrons can be easily computed, hence the experimental results can be compared to quantitative theoretical predictions.

In a solid, positrons predominantly annihilate with outer electrons, i.e., from conduction and valence bands (see Fig. 1). The analysis of the low probability events occurring from annihilation with the core electrons is not feasible in a traditional, single-detector Doppler-broadening setup [Fig. 2(a)] due to the high level of the background. This difficulty can be overcome in a two-detector system [Fig. 2(b)] detecting

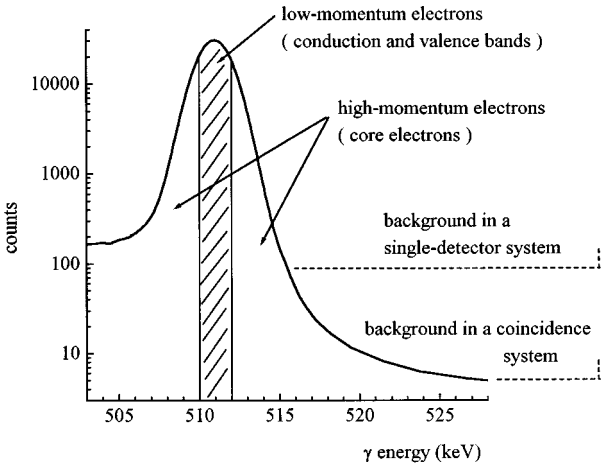

FIG. 1. Typical shape of the annihilation line. The γ energy is related to the momentum of an electron-positron pair as follows: $E_\gamma = mc^2 - \frac{1}{2}E_B \pm \frac{1}{2}p_z c$. The high level of background in a single detector system does not allow one to measure the momentum distribution for large values of the momentum, i.e., large E_γ; see Fig. 2(a). Reduction of the background may be achieved in a coincidence setup; see Fig. 2(b). The actual line shape of Si with voids was used, with a total of 1×10^7 counts.

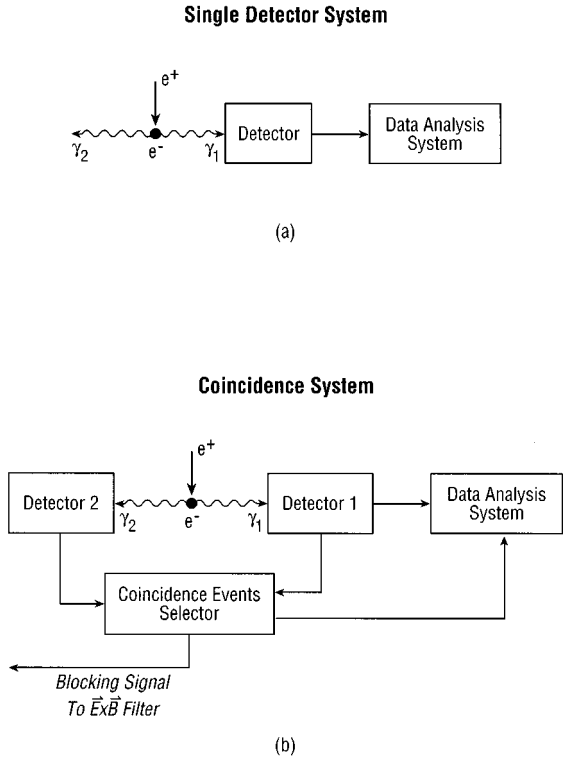

FIG. 2. Block diagrams of the systems used in Doppler-broadening spectroscopy of positron annihilation radiation: (a) a traditional single detector setup in which only one out of the two γ rays is detected and (b) coincidence setup selecting only events in which both γ rays have been registered.

both annihilation photons and selecting only simultaneous events, thus eliminating random background counts. The details of the experimental system have been described by Lynn and Goland as early as in 1976.[8] However, the technique has been seldom used until recently.[7] We applied the coincidence technique to study simple and foreign-atom-decorated vacancies in Si, with emphasis on a technologically important issue of the saturation of doping in Si.

II. EXPERIMENT

All data were collected with a variable energy positron beam in order to provide depth resolution as well as eliminate false coincidence with 1.28-MeV γ radiation from the ^{22}Na source of positrons. A BiGeO scintillator was used for coincidence with a standard high-purity Ge detector. The experimental setup was based on the system described by Lynn and Goland.[8] Pile-up counts at the high-energy side of the annihilation line were reduced by gating the positron beam. After each count recorded in the Ge detector, a blocking signal lasting for about 20 μs was applied to an $\mathbf{E}\times\mathbf{B}$ energy selector,[9] thus preventing the arrival of the positrons to the target before the Ge-detector signal is restored to the equilibrium level. Such a procedure is advantageous over the standard pileup rejection (PUR) system used in nuclear instrumentation modules, since, at least in principle, it allows one to discard counts almost immediately following a given count. In addition, it eliminates permanent detector dead time due to the generation of a continuous PUR signal.

Divacancies in Czochralski-grown Si(100) were generated by irradiation at 25 °C with 5-MeV Si ions to a total dose of 8×10^{13} cm^{-2}. Irradiation at such conditions is known to produce undecorated Si divacancies: Si monovacancies are unstable at room temperature.[10] Open-volume defects larger than a divacancy do not form (Holland, El-Ghar, and White showed the resemblance of the annealing behavior of Si irradiated with Si to the behavior found in samples containing Si divacancies.)[11] The Doppler broadening of the positron annihilation line of irradiated Czochralski (Cz) Si and float zone (FZ) Si are identical, thus ruling out the possibility of the decoration of the divacancies with oxygen[12] (present only in Czochralski-grown Si crystals).

Si-containing voids with the size reaching several nanometers was obtained from thick films of Si grown at 450 °C using molecular-beam epitaxy (MBE). The thicknesses of these films exceeded the critical epitaxial length of the crystalline growth.[13] Transmission electron microscopy (TEM) measurements of similar samples showed the existence of voids in layers beyond the critical epitaxial thickness.[14]

Alternatively, Si-containing voids of comparable sizes were prepared by the exposure to a rf hydrogen plasma of a Si substrate kept at 300 °C. This procedure creates large bubbles filled with hydrogen and subsequent annealing at 700 °C releases H trapped in the voids.[15] Thin Sb-doped Si samples were deposited in a custom MBE system. All were grown at 220 °C at a growth rate of 0.2 Å /s, 50 nm thick, and with 5-nm-thick caps of undoped Si to obtain reproducible surface conditions. Measurements were preceded by methanol cleaning and a 3-min 0.5% HF-acid bath for surface oxide removal, followed by a 1-min H_2O rinse.[16–18]

The same etching procedure was used for the study of hydrogen terminated bonds at the surface of silicon. As-received, float-zone silicon single crystals (resistivity greater than 2000 Ω cm) were used to examine the surface of Si covered with native oxide.

Vacancies in Al were measured in a 99.999% Al foil kept at 500 °C. Vacancies in polycrystalline Cu were generated by pulsed ion-beam melting and subsequent resolidification.

For reference elements, high-purity (at least 99.999%) lumps and foils were used. Defects introduced during manufacturing of these samples were removed by annealing at the temperature approximately equal to 85% of the melting point temperature, i.e., 700 K for Sb and Al. An as-received, i.e., defective, sample of Sb was used as an example of open-volume defects in Sb.

III. RESULTS

A. Identification of elements

Shape variations of the Doppler-broadened spectrum due to the core-electron momentum distribution of different elements is illustrated in Fig. 3. Figure 3(a) depicts an annihilation line shape in several cases of ''defect-free'' (as ''seen'' by positrons) specimens. Only the right-hand side of the peak is shown to eliminate the effect of the high level of background for energies up to 511 keV, caused by the incomplete charge collection in the Ge detector. Photons origi-

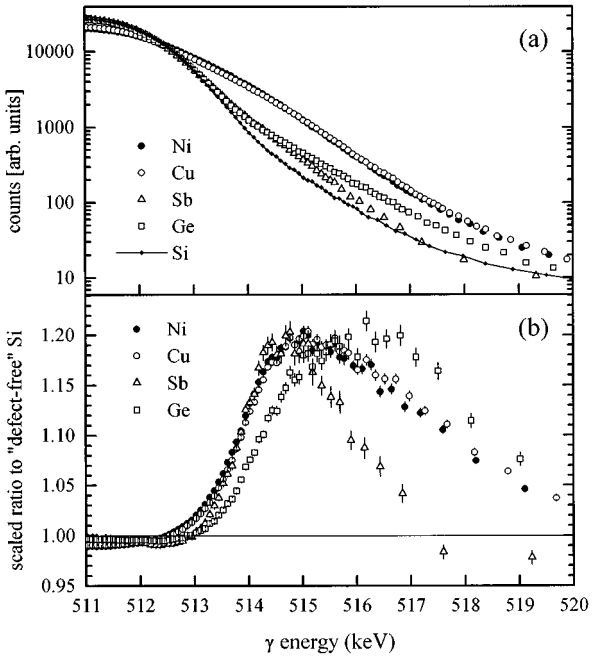

FIG. 3. Annihilation line shape constitutes a signature of an element (a). Variations for large values of E_γ are slightly reduced due to background counts. To obtain a ratio curve, counts for the specimen of interest are divided by counts of a reference element (which here is control Si) for each γ energy. In order to show that the plots differ not only by amplitude but by the shape as well, the plots have been scaled to get the same amplitude of the main peak (b). A smoothing routine was applied here, as well as in the subsequent figures. See Sec. IV for details.

nating from the three-photon decay of positronium are another reason not to analyze the low-energy side of the peak.

Intensities within the range of interest differ by several orders of magnitude and are especially small at γ energies corresponding to core-electron annihilation, i.e., above about 513 keV. To emphasize small changes, intensities are scaled by dividing the counts at a given γ energy by those of a reference element.[19] For Fig. 3(b) pure Si was chosen as the reference element. The choice of the reference material is motivated by the ease of obtaining high-quality single-crystal wafers and because the primary focus of our studies is impurity-vacancy binding in Si. Before the ratio is taken, both spectra are normalized to the total area extending from 505.12 to 516.77 keV. Hereafter, such normalized and scaled plots will be termed ''ratio curves.'' In addition, every ratio curve in Fig. 3(b) is scaled to have equal amplitude at the maximum. This is to emphasize that the curves differ not only in the amplitude but also in the peak positions and the overall shape. The amplitude itself typically cannot be the basis of atom recognition, since for systems with multiple components, it will depend on the fraction of annihilation with other elements present in the specimen.

Figure 3(b) demonstrates ratio-curve variations between different elements. In most cases, the shape of the curves provides unique element identification; see, for example, Sb and Ge. It may happen, however, that the momentum distributions of the core electrons of two distinct elements is indistinguishable within the range of the momentum values tested in this work. Then the corresponding ratio curves are identical. This is the case of Cu and Ni, differing only in the conduction- and valence-band configurations, i.e., low-momentum distribution.

Presentation of the data using ratio curves emphasizes small changes in the annihilation line shape for large values of E_γ, i.e., for large values of momentum of the electrons. Since the count rate at high-γ energy is low, the statistical scattering of experimental points is large. Choosing another way of data presentation may be suitable for the analysis of the contribution at lower values of E_γ. Taking the difference instead of the ratio of the spectra is a possibility.[20]

The high-momentum part of the annihilation line shapes and, consequently, ratio curves can be simulated within an independent-particle model.[19] For the ith shell, the probability of electron-positron annihilation is

$$P_i(E)=\lambda_i(E)/\lambda_{\mathrm{tot}}=\tau\lambda_i(E), \tag{1}$$

where $\lambda_i(E)$ is the fractional annihilation rate, λ_{tot} is the total annihilation rate, and τ is the positron lifetime. Due to technical difficulties in the calculation of the contribution of the conduction and valence electrons to τ, it is convenient to use an experimentally obtained value. Calculations performed by Lynn *et al.*[19] for pure aluminum yielded excellent agreement for $E_\gamma > 516$ keV.

B. Vacancies

In defect-free elements, positrons annihilate from delocalized Bloch states. The introduction of negatively charged or neutral open-volume defects causes positron trapping, i.e., localization of its wave function. The probability of the annihilation of a trapped positron with core electrons is reduced when compared to the annihilation of a delocalized positron. This is because the overlap of the wave function of the core electrons and the trapped positron is reduced. Since the positron is localized, its wave function decreases rapidly with the distance from the trap center. The wave functions of the core electrons, on average, decrease with the increase of the distance to the nucleus. Consequently, the overlap of the wave functions of the localized positron and core electrons is reduced and so is the contribution of the core electrons to annihilation (as opposed to the outer-shell electrons, which are much less susceptible to the reduction to the overlap because they extend to a larger distance from the nucleus).

The reduction of the contribution of the core electrons has been investigated in various pure open-volume defects in Si. Divacancies and amorphous Si were produced using high-energy Si-ion irradiation. Si irradiation eliminated vacancy tieup with foreign atoms, which would occur with a non-Si implant. Si films with voids were obtained from low-temperature (LT) molecular-beam epitaxy layers by growing films thicker than the epitaxial thickness h_{epi}, a critical value above which single-crystalline growth is disrupted and results in a highly defective film.[13] Such films were previously investigated and TEM pictures revealed the existence of voids several nanometers in size.[14] Voids were also created by rf hydrogen plasma exposure of Si and subsequent annealing to drive out the hydrogen trapped in the voids.[15] The defects were identified by the value of the S parameter and their annealing behavior.[12,3,10,21] The S parameter represents the contribution of the conduction and valence bands in the

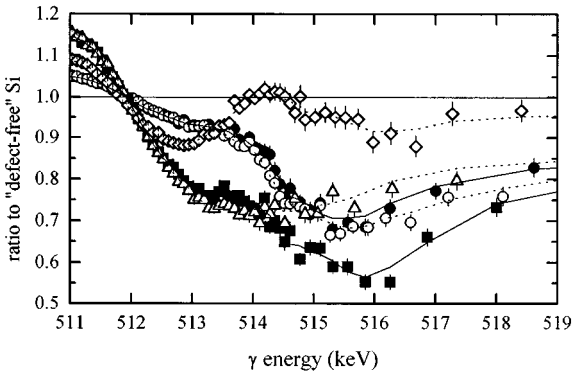

FIG. 4. Pure open volume defects in Si divacancy (●), amorphous (○), void 1 (■) obtained from LT MBE Si ($S=1.09$) scaled to correct for annihilation of delocalized positrons (see Sec. III B, void 2 (Δ) obtained from LT-MBE Si ($S=1.11$), and void 3 (◇) from the exposure to H plasma and subsequent annealing. The smooth lines serve as a guide for the eye only. Defect-free Si was chosen for the reference line shape (see Sec. III A).

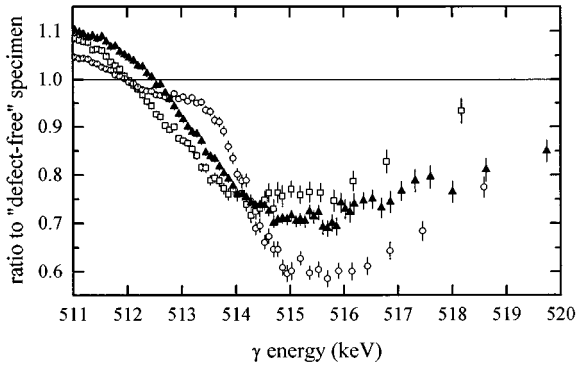

FIG. 5. Pure open volume defects for selected elements: the open volume defect in Sb (□), the Al vacancy (○), and the open volume defect in Cu (▲). the corresponding defect-free specimen was used for the reference time shapes.

annihilation events and is defined as the ratio of counts in the central part of the peak, i.e., from 510.3 to 511.7 keV, to the total number of counts (506.8–515.1 keV). For a silicon divacancy, the generally accepted value of S is ~ 1.04;[12] it is greater for defects larger than divacancies.

The ratio curves corresponding to experimental line shapes for these defects, with respect to the defect-free single-crystal Si, are shown in Fig. 4. The divacancy (full circles) exhibits a minimum centered at about 515.5 keV. In addition, a minimumlike change of the slope around 512.8 keV is observed. Similar minimum or minimumlike slope changes exist in the spectrum of voids in the LT MBE Si sample yielding the S parameter of 1.09 (depicted as full squares in Fig. 4). Another LT MBE sample (plotted as triangles in Fig. 4) reveals only one minimum, centered at 514 keV. The size of the voids in this sample is thought to be larger than in the former one as the value of the S parameter is larger (1.11 compared to 1.09). In the case of the voids observed in Si exposed to H plasma (diamonds in Fig. 4), two minima are observed. The defected layer in this sample is very narrow and is buried immediately below the surface; hence a surface contribution to the spectrum may be expected due to positrons diffusing to the surface and annihilating there. The peak at 514 keV bears a close resemblance to the spectrum of SiO_2 (see Fig. 6 and Sec. III C) and it may originate from H or OH termination of Si bonds at the surface. Surprisingly, the ratio curve of amorphous Si is only slightly different from the divacancy curve.

The complex functional form of the ratio curves indicates that a defect cannot be uniquely characterized using a single-number parameter, such as the S parameter or a W parameter (W is defined as the ratio of the integrated counts in an arbitrary selected range of γ energy to the total counts). Two defects can maintain the same S parameter, while having different values of W parameters. The relationship depends on the selection of the range of γ energy used in the calculation of the W parameter. Therefore, an analysis of the whole ratio curve provides a more complete way of a defect characterization than an analysis of the S or W parameters.

At γ energy above 520 keV, the spectra are dominated by the system background and the ratio curves converge to unity level. Our plots were truncated above $E_\gamma = 519$ keV to avoid suggesting that the high-momentum core contributions are identical. The use of a coincidence system based on two Ge detectors will produce a much lower level of background and will allow one to investigate the contribution of larger values of momentum.[22]

Not all positrons annihilate after being trapped at defect sites: some may annihilate as delocalized Bloch states. Therefore, the measured ratio curves of defects are not necessarily the spectra of the corresponding defects only. In order to obtain the exact ratio curves in cases when positron trapping at the defects is not saturated, it is necessary to correct the plots according to the ratio of positron-annihilation rates at the defects and as delocalized states:

$$\frac{(\text{pure defect})}{(\text{defect-free})} = \frac{1}{b}\left(\frac{(\text{measured defect})}{(\text{defect-free})} - a\right), \qquad (2)$$

where a and b are the annihilation fractions corresponding to positrons that are delocalized and localized at defects, respectively. Positron lifetime measurements may be used to obtain the ratios of the annihilation rates.[14] Alternatively, similar information can be obtained from 2D ACAR data. The 2D ACAR spectrum in p_x and p_y momentum space, collected at γ energies corresponding to the void signal, consists of two components (not shown). The first one is a well-known spectrum of Si single crystal, i.e., of delocalized positrons, and the second one, very narrow, is the spectrum of the void. Gradual subtraction of the bulk component from the combined signal of the voids and the single crystal Si, until the characteristic features of the bulk disappear, yields the ratio of annihilation rates for the two annihilation channels.[23] We performed the above procedure for the sample with voids, for which the S parameter was equal to 1.09 at $E_\gamma = 3.5$ keV and obtained $13 \pm 2\%$ of the annihilation from delocalized positrons and $87 \pm 2\%$ from positrons trapped at the voids. The ratio curve of the voids in that sample (shown in Fig. 4 as full squares) was corrected to remove the effect of annihilation of nonlocalized positrons. The larger voids characterized by S parameter of 1.11, as well as voids created through the exposure to H plasma, were

not corrected for the effect of annihilation of delocalized positrons. The ratio curves of divacancies and amorphous Si were considered to correspond to saturation trapping of positrons at defects because a saturation plateau was observed in the plot of S vs positron energy (not shown).

Although no theoretical predictions of the electronic shell contribution to the momentum distribution have been published for γ energies below 513.6 keV, Alatalo *et al.* calculated the distribution for levels $2s$, $2p$, and $3s$ in Si in the range 513.6 keV $<E_\gamma<$518.9 keV.[7] Electron and positron wave functions in a single-particle approximation were used and the short-range electron pileup at the positron was taken into account using an enhancement factor calculated using the local-density approximation.

Analysis of the single electronic-shell contribution indicates that a decrease in the $2p$ level reduces the momentum distribution for $E_\gamma>516$ keV, suggesting a correlation between the experimentally observed valley at 515.5 keV and a decrease in the annihilation rate with $2p$ electrons. The decrease is caused by a reduction of the positron and $2p$ electron overlap due to the increased separation between them. Because of the unavailability of theoretical calculations for low momentum (i.e., 511 keV $<E_\gamma<$513.6 keV), the origin of the valleylike slope variations around 513 keV is not clear, although extrapolation of the calculations performed by Alatalo *et al.* implies that a decreased number of annihilation with $2s$ electrons might be responsible for the effect. This is contrary to the expectation of a negligible contribution to the annihilation from $2s$ electrons due to the Coulombic repulsion between the nucleus and the positron at $2s$ orbital positions. However, according to the same calculations by Alatalo *et al.*, the overlap of the wave functions of a positron and $2s$ electrons can be detected. The partial annihilation rate for the $2s$ shell is only about three times smaller than for $2p$ ($\lambda_{2s}=0.034$ ns^{-1} and $\lambda_{2p}=0.106$ ns^{-1}) and the $2s$ shell contribution may be observable.

The presence of a positron inside a vacancy may induce some relaxation of the surrounding atoms, as well as modify the wave functions of the electrons. Therefore the ratio curves of the defects plotted above may differ slightly from the actual ratio curves. This is an intrinsic limitation of the method, which could be corrected with the use of self-consistent calculations. The difference between the divacancy and void signals needs further theoretical investigation.

A similar decrease of the density of high momentum core electrons in samples with open volume defects has been observed in specimen other than Si: aluminum, copper, and antimony (Fig. 5). Vacancies in aluminum lead to a valley and valleylike slope changes in the structure of the ratio curve similar to those obtained in silicon and this could be explained by the identical configuration of the core electrons. The core structure of copper and antimony, on the other hand, differs substantially from silicon and so do the ratio curves of the corresponding vacancies. Similar reductions in the annihilation with core electrons are expected to be a general feature observed in pure open-volume defects.

C. Surface termination

The surface of a specimen can, in concept, be considered as a large defect, and in many applications its presence is important. In studies involving shallow layers, due to positron diffusion and subsequent trapping at the surface, the surface contribution alters the measured ratio curves. Therefore, a basic understanding of the silicon surface is important.

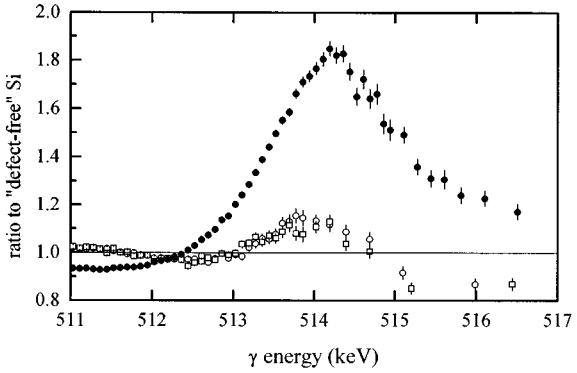

FIG. 6. Ratio curves of Si surfaces for various orientations and surface termination: HF-etched Si(111) (○); HF-etched Si(100) (□), not treated, i.e., oxidized, and Si(111) (●). The unity line represents the defect-free Si.

When stored in air, like most materials, silicon easily oxidizes. The corresponding ratio curve, with respect to the bulk, defect-free Si, is shown in Fig. 6. Unlike the case of a vacancy-like defect in Si, the low-momentum contribution for $E_\gamma<512$ keV is reduced. A sharp peak centered at about 514 keV appears. The huge magnitude of the peak often prevents a correct analysis of the defects in a nearby subsurface layer. Therefore, it is often necessary to remove the oxide film, which is usually done by chemical etching in aqueous hydrofluoric acid, followed by rinsing in water.[16–18] It has been established that during this process dangling bonds of silicon get terminated with hydrogen and hydroxide.[24] The corresponding ratio curves for HF-etched Si(111) and Si(100) are shown in Fig. 6. Within experimental errors, they are identical for both crystal orientations [both curves with respect to defect-free Si(111)], but no dependence on crystal orientation could be found for defect-free Si. A significant reduction of the magnitude of the peak centered at 514 keV is observed in the HF-acid etched samples. This indicates the disappearance of the surface oxide. Because the origin of the peak is thought to be oxygen related, its remnant could be explained by trace amounts of hydroxide covering the surface. This result agrees well with ir absorption experiments, where both OH and H terminated bonds were found after HF etching.[24]

D. Defects in Si doped with Sb

Using a molecular-beam epitaxy, it is possible to dope silicon to concentrations exceeding the limit of solid solubility. For antimony,[25] the solid solubility reaches a maximum value of 7×10^{19} cm^{-3} at 1300 °C and decreases to about 2×10^{19} cm^{-3} at 700 °C. At temperatures used in LT MBE (200 °C–300 °C), the solubility limit is even lower.

Doping of silicon with antimony using MBE linearly increases the net concentration of electrical carriers up to about 7×10^{20} cm^{-3} and a further increase in the dopant concentration does not show a corresponding increase in the carrier

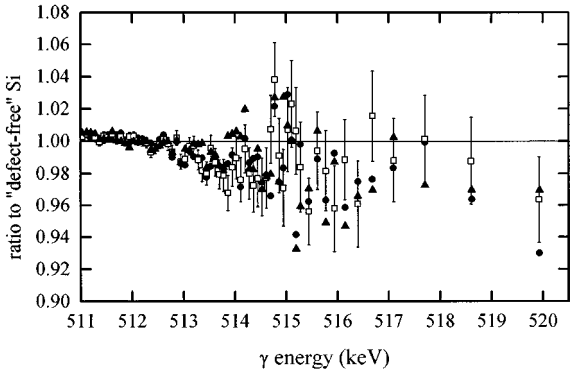

FIG. 7. Ratio curves for bulk Si highly doped with Sb (●), As (□), and P (▲), with respect to high-resistivity float zone Si(111) ($\rho > 5000\ \Omega$ cm). All wafers were obtained from a commercial vendor. The energy of positrons was selected to be above 20 keV to prevent the diffusion of positrons to the surface. For clarity, the error bars were plotted only in the case of Si:As.

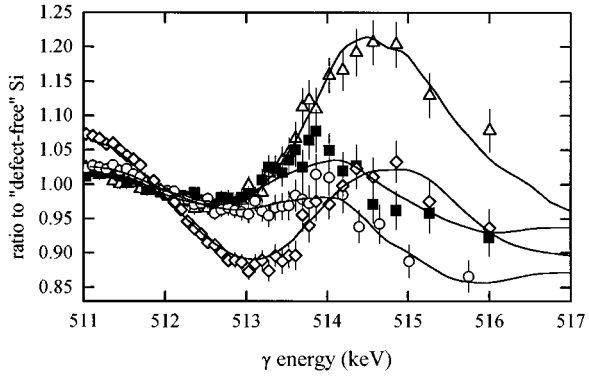

FIG. 8. Si doped with Sb for various dopant concentrations: 9.8×10^{19} cm^{-3} (○), 5×10^{20} cm^{-3} (□), 1.1×10^{21} cm^{-3} (△), and 2.4×10^{21} cm^{-3} (◇). The open symbols represent experimental data and the lines best fits obtained as linear combinations of the expected constituents. The data were truncated above 517 keV to remove uncertainties associated with insufficient statistics and systematic errors of the background; see Sec. IV for a discussion.

concentration.[26] Walukiewicz has shown[27] that at high doping concentrations the Fermi statistics of the electron and hole gas is degenerated. This lowers the formation energy of native defects, which, when activated, can compensate shallow dopants. Adler *et al.* have proposed that the creation of a new defect, Sb tied to a monovacancy, in the regime of high doping levels and acting as a compensating acceptor is responsible for the saturation of the concentration of electrical carriers.[28] The later hypothesis can be verified with the approach described in the earlier sections. The structure of the Sb core electrons is different from that of Si. Consequently, the momentum distributions of the core electrons of Sb and Si are different. The formation of the antimony-vacancy complex is hence expected to be observable in the annihilation spectrum as an enhancement of the Sb features.

It is important to realize that Sb can be detected using this technique only if it is tied with an open-volume defect, which, in addition, must be negatively charged or neutral. Otherwise positrons will not localize near it. For linear doping regime, all substitutional Sb atoms are ionized at room temperature and carry a positive charge. Therefore they repel positrons. We confirmed this model experimentally for Sb, as well as other group-V donors, namely, P and As, for dopant concentrations estimated to be below 10^{19} cm^{-3}. Commercially available wafers were used. The data are plotted in Fig. 7 and all of the presented ratio curves are in agreement with a unity curve representing high-purity single-crystal silicon. Small reductions for $E_\gamma < 514$ keV, if any, although within the range of experimental error bars, might be due to vacancylike behavior.

To verify whether a complex of Sb tied to a vacancy is produced at high doping levels, a set of four LT MBE samples was grown: in the linear regime 9.8×10^{10} and 5×10^{20} cm^{-3} and above the saturation level 1.1×10^{21} and 2.4×10^{21} cm^{-3}. The experimental ratio curves with respect to defect-free Si are plotted in Fig. 8. The ratio curves corresponding to the lowest two concentrations of antimony resemble the ratio curve of the Si divacancy (compare to Fig. 9). The 1.1×10^{21}-cm^{-3} sample exhibits a peak centered at 514.5 keV. The peak position coincides with the position of a maximum observed in the ratio curve of defect-free antimony to control silicon, suggesting the contribution of Sb in the defects (see Fig. 9). If Sb is tied to a vacancy and is the compensating defect present in the $n_{\mathrm{Sb}} = 1.1\times10^{21}$ cm^{-3}, the corresponding ratio curve should also contain the momentum distribution of the electrons of Si atoms surrounding a vacancy in Si lattice. After all, neglecting relaxation effects, the complex of Sb tied to a vacancy differs from the undecorated Si vacancy only by a replacement of one Si atom with Sb. In order to prove it, we fitted each plot as a linear combination of annihilation spectra corresponding to the atoms surrounding the vacancy in the complex of Sb tied to a vacancy. The spectrum of the Si divacancy was used to model the Si atoms and the spectrum of defect-free Sb to model Sb atoms. It should be stressed that the whole spectra, i.e., 511 keV $< E_\gamma <$ 517 keV, were used for the fitting. This means that the contributions of both high- and low-momentum electrons were taken into account. Since the distribution of the low-momentum part (which corresponds to the conduction and valence electrons) is strongly dependent on the nearest-neighbor atoms, the overlap of the electron and positron wave functions is different for defective and defect-free

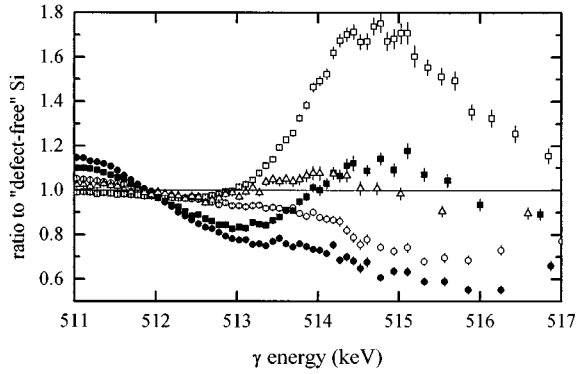

FIG. 9. Ratio curves for the divacancy (○) and a void (●) in Si, defect-free (□) and defective (■) Sb, and the HF-etched surface of silicon (△), i.e., expected components in silicon doped with antimony layers.

TABLE I. Results of the fitting of the Si:Sb ratio curves as a linear combination of Si vacancy, Si void, defect-free Si, defect-free Sb, Sb vacancy, and the HF-treated Si surface. NA denotes not applicable, i.e., a satisfactory fit could be obtained using the coefficient set to zero.

n_{Sb} cm^{-3}	*a* (Si divacancy)	*b* (Si void)	*c* (defect-free Si)	*d* (atoms of defect-free Sb)	*e* (atoms of defective Sb)	*f* (surface of HF-etched control Si)
9.8×10^{19}	0.51(7)	NA	0.26(14)	0.06(4)	NA	0.17(12)
5×10^{20}	0.10(7)	NA	0.35(14)	0.03(4)	NA	0.52(12)
1.1×10^{21}	0.38(4)	NA	0.20(5)	0.42(2)	NA	NA
2.4×10^{21}	NA	0.14(9)	0.35(16)	0.01(6)	0.50(12)	NA

specimen. The spectrum of defect-free Sb was used instead of defective Sb because no satisfactory fit could be obtained using defective Sb. The choice is governed by the localization of the positron inside the vacancy, but a thorough understanding of which component is needed is missing. Theoretical investigation of the issue is being conducted, but no consensus has been reached so far.[29] In the linear combination we also included a term corresponding to silicon atoms as seen in defect-free Si to account for the annihilation of nonlocalized positrons in Si (in a defect free specimen all positrons annihilate from nonlocalized states). Because the thickness of the investigated layer (50 nm) is comparable to the positron diffusion length [200 nm for defect-free Si (Ref. 30)], some positrons diffuse back to the surface and annihilate there. It is therefore necessary to add a term corresponding to the surface. We used the spectrum of the surface of defect-free Si, etched in HF acid the same way as the other samples. It was assumed that the surface termination is identical for all samples because the growth of the investigated layers in all samples was followed by a deposition of a thin epitaxial film of pure silicon. For the $n_{Sb}=2.4\times10^{21}$ cm^{-3} sample, the spectra of Si voids and of as-received (defective) antimony were needed for a satisfactory fit. The fitting of the ratio curves was achieved with the formula

$$r(E)=a\,\mathrm{Si}_{\mathrm{vacancy}}(E)+b\,\mathrm{Si}_{\mathrm{void}}(E)+c\,\mathrm{Si}(E)+d\,\mathrm{Sb}(E)+e\,\mathrm{Sb}_{\mathrm{vacancy}}(E)+f\,\mathrm{Si}_{\mathrm{surface\ (HF\ etched)}}, \quad (3)$$

where $r(E)$ is the experimental value of a ratio curve at energy E and the fitting coefficients satisfy the normalization constraint: $a+b+c+d+e+f=1$. The Marquadt-Levenberg least-squares nonlinear fitting routine was applied to unmodified experimental data weighted by statistical errors. The fitted curves are shown in Fig. 8 as solid lines. The experimental curves were smoothed using the variable averaging algorithm described in Sec. IV. All fitted curves show qualitative agreement with the experimental data. The fitted coefficients are shown in Table I. The coefficients in each row add to unity and they should be understood as the fractions of annihilation only. The entries NA (not applicable) denote that the corresponding component was not needed for a satisfactory fit. In such cases, the coefficient was set to zero if a full-parameter fit yielded a value of zero (within the error bar). The fit was then repeated to reduce the uncertainties of the coefficients. To extract the absolute values of the concentration of each defect or defect component (e.g., Sb being a part of the Sb-vacancy complex), the corresponding coefficient should be multiplied by the total number of defects detected by positrons. This can be obtained from the positron diffusion length, which, in the absence of a built-in electric field, decreases with the increase in defect concentration. The diffusion length is obtained by solving a diffusion-annihilation equation[1] applied to the sample partitioned into several layers characterized by a value of the *S* parameter. Fitting the model to the experimental *S* vs *E* profile allows one to extract the diffusion length and then to calculate the defect concentration. A computer program, known as VEPFIT, developed by van Veen *et al.*,[31] was used to solve the diffusion-annihilation equation.

The total defect concentrations extracted with the above procedure are listed in Table II. The trapping rate of 5×10^{14} s^{-1} was used to estimate the defect concentration from the fitted diffusion length.[32] The sensitivity limit of the detection of defects was estimated to be 3×10^{18} cm^{-3}. A procedure described by Asoka-Kumar *et al.* was used and assuming $d=50$ nm, $S_{\mathrm{surf}}=1.028$ (as measured for the sample with $n_{\mathrm{sb}}=9.8\times10^{19}$ cm^{-3}) and $S_{\mathrm{defect}}=1.035$ (corresponding to Si divacancy, since the divacancy is the dominating defect in this sample: see the following text).[33]

All samples turned out to be defective, including the lowest dopant concentration, indicating the creation of open-volume defects during the LT MBE growth with a doping level of at least 9.8×10^{19} cm^{-3}. The measurements were conducted at elevated temperature (100 °C) in order to eliminate the electric field of trapped charges. Such field would modify the positron diffusion length and consequently the concentration of the defects. The existence of defects in all samples should not be a surprise, since it has been already established that LT MBE-grown Si exhibits the formation of open-volume defects before reaching h_{epi}, the limit of epitaxial growth.[34] It is also known that doping decreases h_{epi}, causing the formation of defects at an earlier stage of the growth. Radamson *et al.* showed[35] that doping Si with Sb decreases h_{epi} from 1000 to 25 Å for Sb concentration changing from 2×10^{20} to 2×10^{21} cm^{-3}. Since h_{epi} is strongly dependent on the growth conditions, it is difficult to directly apply these results to our samples. Reflection high-energy

TABLE II. Defect concentrations in Si:Sb layers obtained through the solution of the diffusion-annihilation equation.

N_{sb} (cm^{-3})	n_{defect} (cm^{-3})	$n_{\mathrm{defect}}/n_{\mathrm{sb}}$
9.8×10^{19}	$1.3(4)\times10^{19}$	0.13(4)
5×10^{20}	$1.6(4)\times10^{19}$	0.03(1)
1.1×10^{21}	$1.3(2)\times10^{20}$	0.11(2)

electron diffraction data obtained during the growth of our samples showed well-defined patterns at the three lowest Sb concentrations and the disappearance of the pattern during the growth at the highest Sb concentration. Therefore, we concluded that only the sample with the highest doping level (2.4×10^{21} cm^{-3}) exceeded the limit of epitaxial growth. The analysis of the defect character is included in the following paragraphs.

Similarly, the results from Table I show that none of the samples are defect-free. A defect-free sample would yield all the coefficients equal to zero, except for c and f, i.e., 100% of annihilation would occur from the delocalized states of positrons in the solid or positrons trapped at the surface. Clearly this is not the case for any of the samples under study.

In the case of the two lowest concentrations of the dopants, both in the linear range of dopant activation, the Si divacancy was found to be the dominating defect. No or almost no Sb was detected [0.06(4) and 0.03(4) for $n_{\mathrm{Sb}}=9.8\times10^{19}$ and 5×10^{20} cm^{-3}, respectively]. Remembering that electrically activated Sb atoms cannot trap positrons, this is consistent with the data of electrical activation of the donors, where $\sim$100% of Sb was activated for $n_{\mathrm{Sb}}<7\times10^{20}$ cm^{-3}.

Increasing the dopant concentration to 1.1×10^{21} cm^{-3} causes a saturation of the electrical activity, i.e., some Sb atoms do not reside as substitutional donors. Instead, according to the model of Adler *et al.*, they tie up with monovacancies.[36] When a positron is trapped in an open volume adjacent to a Sb atom, its wave function overlaps with the wave functions of Sb electrons. Consequently, the shape of the corresponding Doppler-broadened annihilation line is determined by the distribution of momentum of Sb electrons. It becomes possible, then, to detect a ''Sb shape'' in the ratio curve. Indeed, the contribution of defect-free Sb to annihilation was observed (see the coefficient d in Table I), meaning that Sb is a constituent of the principal defect in the sample. The value of $a=0.38(4)$ for $n_{\mathrm{sb}}=1.1\times10^{21}$ cm^{-3}, i.e., the fraction of annihilation events with electrons belonging to Si atoms surrounding a Si vacancy (due to the lack of a reference sample containing Si monovacancies, we used the spectrum of a Si divacancy and assumed a close resemblance between the two), implies that positrons trapped at the defect also annihilate with Si electrons, as expected. This suggests that the principal defect contains a vacancy. Since a Si void signal was not detected (see coefficient b), the possibility of Sb being tied to a void can be excluded.

A more detailed characterization of the defect based on the fitted coefficients, i.e., establishing the number of Sb and Si atoms surrounding the vacancy, is impossible at this point due to two reasons. First, the rates of annihilation of positrons with Si and Sb when trapped at the complex of Sb tied to a vacancy are not known, although theoretical calculations could resolve this problem. Second, Sb tied to a vacancy is not the only defect contributing to the coefficient a. Pure silicon divacancies, certainly present in the specimen, may also contribute and an independent estimate of their number is necessary.

In spite of this, single Sb tied to a vacancy is proposed as the compensating acceptor and supporting evidence arises from extended x-ray-absorption fine-structure measurements[36] (data collected for $n_{\mathrm{Sb}}=1.5\times10^{21}$ cm^{-3}). No Sb-Sb bonding was detected, which rules out the possibility of Sb clustering.

The $n_{\mathrm{Sb}}=2.4\times10^{21}$ cm^{-3} sample exhibits a totally different behavior than the first sample in the saturation regime of carrier concentration, i.e., $n_{\mathrm{Sb}}=1.1\times10^{21}$ cm^{-3} (see Fig. 8). The contribution of high-momentum electrons is substantially reduced. The decomposition analysis, analogous to the one described above, revealed the existence of another kind of defect since it was impossible to obtain a satisfactory fit using the following components: Si surface, Si divacancy, and a void in Si lattice, Sb atoms in defect-free specimen and Si atoms as in defect-free Si. The addition of a defective, but high-purity, antimony as a new constituent in the fitting produced a reasonably good fit. Since open-volume defects in the Sb lattice may resemble open-volume defects at the Sb-Si interface of antimony precipitates in Si, it is possible that Sb-vacancy complexes combine and form precipitates for $n_{\mathrm{Sb}}=2.4\times10^{21}$ cm^{-3}. The presence of Sb precipitates is understandable, considering the huge (5% atomic fraction) amount of Sb in the Si lattice for this sample. This interpretation is not unique. The existence of another defect of Sb tied to an open volume must be considered too. The simultaneous appearance of Si voids and defective Sb, at the expense of Si divacancies and defect-free Sb, seems to support this hypotheses; see Table I. In addition, the void signal has two possible interpretations: as open volume defects at the boundaries of Sb precipitates or as pure voids in the Si lattice.

IV. DISCUSSION OF ADVANTAGES AND DISADVANTAGES OF THE CORE COMPONENT ANALYSIS

The measurements of high-momentum core electrons do not suffer from small instabilities of the Ge-detector energy resolution, which is a common problem in standard Doppler-broadening measurements. This is because the relative changes observed in the counts of the annihilation line are typically much larger at the γ energy far from the peak centroid (511 keV) than at the centroid itself. This was verified experimentally by an intentional degrading of the instrumental resolution of the Ge detector from the full width at half maximum equal to 1.57 to 1.6 keV. No change in the core shape was observed.

It should be mentioned that by using positron annihilation data, it is impossible to completely separate the contribution from core electrons and conduction-band–valence-band electrons. This is an intrinsic problem of the normalization, since the change in the count rate at the central part of the line shape causes an opposite change in the tails. It is the variations in the overall shape of the ratio curve that contain unique information about the changes in the momentum distribution of electrons.

The analysis presented above for the high-momentum contribution to annihilation events does not take into account the possibility of positron annihilation with electrons other than from the first Brillouin zone (umklapp processes.[37]) Mijnarends[38] calculated the umklapp correction to the momentum density in copper and the calculations agree with the

positron annihilation data.[37] However, the umklapp contribution is excepted to be small.

Since the count rate at the tails of annihilation line shapes is very low compared to the central part of the peak, the corresponding errors for $E_\gamma > 514$ keV are quite large. In order to extract physical behavior it was necessary to apply a smoothing routine. The algorithm we used, hereafter called variable averaging, performed averaging of the counts of several adjacent channels of the multichannel analyzer if the calculated statistical errors were exceeding a given threshold, typically 3%. The value of the average was used to generate a data point placed at E_γ determined as the centroid of the channels taken to calculate the average. As E_γ increases and the counts in each channel decline, the number of channels needed for the averaging increases. This causes a gradual reduction in the density of the averaged data points when E_γ increases. In the plots, the enlarged spacing between the points along the abscissa reflects the statistical errors of the counts in the ordinate. Such a smoothing procedure hides subtle changes in the spectra and one should be aware of the uncertainties associated with high energy ($E_\gamma > 517$ keV) points of the ratio curves. To test the reliability of the algorithm, a high statistics data (1.5×10^7 counts per spectrum) was collected. Within the allowed error of 3%, the variable averaging performed for 2×10^6 counts per spectrum, yielded excellent agreement for $E_\gamma < 517$ keV (not shown). Not enough data were collected for testing for larger values of E_γ. The variable averaging algorithm is advantageous over the commonly used Gaussian convolution, since the large width of the Gaussian, necessary for proper smoothing in the tails of the annihilation line shape, would deform the central part of the line shape.

At sufficiently high-γ energies, in spite of the use of a coincidence setup, background effects become increasingly important. The main consequence is convergence of the counts at the tails to a constant level determined by the background level. This behavior might mistakenly suggest that electrons of all elements have identical distribution at very high momentum (corresponding to $E_\gamma > 520$ keV). To avoid confusion, we limited the data analysis to $E_\gamma < 520$ keV or even smaller energies in selected cases. The experimentally observed background is not caused by random counts from unknown sources since they are rejected by the coincidence setup and cannot be simply subtracted from the experimental data. It originates from pileup events and has not been eliminated completely in spite of the use of the PUR system based on the beam gating described in Sec. II, presumably due to time delays in the electronic part of the system. The background problem might be removed numerically using deconvolution with an effective background function.[39,40]

V. CONCLUSION

We have shown that the chemical variations of defects in a specimen can be identified by measuring the contributions of core electrons to the annihilation line shape. The measured spectra can be described as a linear combination of reference elements or known defects. Direct analysis of the coefficients of the decomposition requires theoretical modeling of trapping rates or positron lifetime measurements. Depth-resolved identification of defects is possible in a coincidence setup installed at a variable energy positron beam.

The technique has been applied to examine open volume defects in Si. In particular, a reduction in the amount of overlap of a localized positron and core-electrons wave functions in the case of pure divacancies, as opposed to delocalized wave functions of positrons in defect-free Si, has been observed. Sb tied to a vacancy has been shown to be the defect responsible for the saturation of the electrical activity in Si highly doped with Sb.

ACKNOWLEDGMENTS

The authors wish to thank O. W. Holland for the preparation of the samples with Si divacancies and amorphous Si using Si ion implantation and H. J. Stein for supplying the Si sample with voids created by hydrogen plasma exposure. This work was supported in part by U.S. Department of Energy under Contract No. DE-AC02-76CH00016.

[1] P. J. Schultz and K. G. Lynn, Rev. Mod. Phys. **60**, 701 (1988).

[2] M. J. Puska and R. M. Nieminen, Rev. Mod. Phys. **66**, 841 (1994).

[3] P. Asoka-Kumar, K. G. Lynn, and D. O. Welch, J. Appl. Phys. **70**, 4935 (1994).

[4] A. Vahanen and K. Rytsölä, in *Positron Solid-State Physics*, Proceedings of the International School of Physics ''Enrico Fermi,'' Course LXXXIII, Varenna, 1981, edited by W. Brandt and A. Dupasquier (North-Holland, Amsterdam, 1983), p. 659.

[5] S. Berko, in *Positron Anniliation, Proceedings of the 5th International Conference on Positron Annihilation, Lake Yamanaka, Japan 1979*, edited by R. R. Hasigutz and K. Fujiwaza (Japan Institute Met., Tokyo, 1988), p. 65.

[6] K. G. Lynn, in *Positron Solid State Physics* (Ref. 4), p. 609.

[7] M. Alatalo, H. Kauppinen, K. Saarinen, M. J. Puska, J. Mäkinen, P. Hautojärvi, and R. M. Nieminen, Phys. Rev. B **51**, 4176 (1995).

[8] K. G. Lynn and A. N. Goland, Solid State Commun. **18**, 1549 (1976).

[9] A. P. Mills, Jr., Phys. Rev. Lett. **50**, 671 (1983).

[10] G. D. Watkins, in *Deep Centers in Semiconductors. A State-of-the-Art Approach*, edited by S. T. Pantelides (Gordon and Breach, New York, 1992), p. 177.

[11] O. W. Holland, M. K. El-Ghor, and C. W. White, Appl. Phys. Lett. **53**, 1282 (1988).

[12] B. Nielsen, O. W. Holland, T. C. Leung, and K. G. Lynn, J. Appl. Phys. **74**, 1636 (1993).

[13] D. J. Eaglesham, H.-J. Gossmann, and M. Cerullo, Phys. Rev. Lett. **65**, 1227 (1990).

[14] D. D. Perovic, G. C. Weatherly, P. J. Simpson, P. J. Schultz, T. E. Jackman, G. C. Aers, J.-P. Noël, and D. C. Houghton, Phys. Rev. B **43**, 14 257 (1991).

[15] P. Asoka-Kumar, H. J. Stein, and K. G. Lynn, Appl. Phys. Lett. **64**, 1684 (1994).

[16] W. Kern and D. A. Puotinen, RCA Rev. **31**, 187 (1970).
[17] D. J. Monk and D. S. Soane, J. Electrochem. Soc. **140**, 2339 (1993).
[18] M. Niwano, Y. Kimura, and N. Miyamoto, Appl. Phys. Lett. **65**, 1692 (1994).
[19] K. G. Lynn, J. E. Dickman, W. L. Brown, M. F. Robbins, and E. Bonderup, Phys. Rev. B **20**, 3566 (1979).
[20] I. K. MacKenzie, in *Positron Solid State Physics* (Ref. 4), p. 196.
[21] Sjoerd Roorda, in *Materials Synthesis and Processing Using Ion Beams*, edited by R. J. Culbertson, O. W. Holland, K. S. Jones, and K. Maex, MRS Symposia Proceedings No. 316 (Materials Research Society, Pittsburgh, 1994), p. 159.
[22] J. R. MacDonald, K. G. Lynn, R. A. Boie, and M. F. Robbins, Nucl. Instrum. Methods **153**, 189 (1978).
[23] J. P. Peng and K. G. Lynn (unpublished).
[24] M. Niwano, J. Kageyama, K. Kurita, K. Kinashi, I. Takahashi, and N. Miyamoto, J. Appl. Phys. **76**, 2157 (1994).
[25] F. A. Trumbore, Bell Syst. Tech. J. **39**, 205 (1960).
[26] H.-J. Gossmann, F. C. Unterwald, and H. S. Luftman, J. Appl. Phys. **73**, 8237 (1993).
[27] W. Walukiewicz, Phys. Rev. B **50**, 5221 (1994).
[28] D. L. Adler, J. D. Chadi, M. A. Marcus, H.-J. Gossmann, and P. H. Citrin, Bull. Am. Phys. Soc. **40**, 396 (1995).
[29] M. Alatalo and V. J. Ghosh (private communication).
[30] E. Soininen, J. Mäkinen, D. Beyer, and P. Hautojärvi, Phys. Rev. B **46**, 13 104 (1992).
[31] A. van Veen, H. Schut, J. de Vries, R. A. Hakvoort, and M. R. Ijpma, in *Positron Beams for Solids and Surfaces*, edited by Peter J. Schultz, Guiti R. Massoumi, and Peter J. Simpson, AIP Conf. Proc. No. 218 (American Institute of Physics, New York, 1990), p. 171.
[32] P. Mascher, S. Dannefaer, and D. Kerr, Phys. Rev. B **40**, 11 764 (1989).
[33] P. Asoka-Kumar, H.-J. Gossmann, F. C. Unterwald, L. C. Feldman, T. C. Leung, H. L. Au, V. Talyanski, B. Nielsen, and K. G. Lynn, Phys. Rev. B **48**, 5345 (1993).
[34] Cs. Szeles, P. Asoka-Kumar, K. G. Lynn, H.-J. Gossmann, F. C. Unterwald, and T. Boone, Appl. Phys. Lett. **66**, 2855 (1995).
[35] H. H. Radamson, M. R. Sardela, Jr., L. Hultman, and G. V. Hansson, J. Appl. Phys. **76**, 763 (1994).
[36] D. L. Adler, D. J. Chadi, M. A. Marcus, S. Schuppler, H.-J. Gossmannm, and P. H. Citrin (unpublished).
[37] S. Berko, in *Positron Solid State Physics* (Ref. 4), p. 64.
[38] P. E. Mijnarends, Physica (Utrecht) **63**, 235 (1973).
[39] Y. Kong and K. G. Lynn, Nucl. Instrum. Methods. Phys. Res. Sect. A **302**, 145 (1991).
[40] D. T. Britton, P. Bentvelsen, J. De Vries, and A. Van Veen, Nucl. Instrum. Methods Phys. Res. Sect. A **273**, 343 (1988).